3D printing of PEEK/HAp scaffold for medical bone implant

Bankole I. Oladapo*[,1,4], S. A. Zahedi[1], Sikiru O. Ismail[2], Francis T. Omigbodun[3], Bowoto Oluwole[1],
Mattew A. Olawumi[1], Musa A. Muhammad[4]

[1] *School of Engineering and Sustainable Development, De Montfort University, Leicester, UK*
[2] *Centre for Engineering Research, School of Physics, Engineering and Computer Science, University of Hertfordshire, UK*
[3] *Mechanical Engineering, Loughborough University, UK*
[4] *Faculty of Engineering, Environment and Computing, Coventry University, UK*

**Corresponding author: e-mail: Bankole.Oladapo@dmu.ac.uk*

Abstract

The major drawback associated with PEEK implants is their biologically inert surface, which caused unsatisfactory cellular response and poor adhesion between the implants and surrounding soft tissues against proper bone growth. In this study, polyetheretherketone (PEEK) was incorporated with Calcium Hydroxyapatite (cHAp) to fabricate a PEEK/cHAp biocomposite, using the fused deposition modeling (FDM) method and a surface treatment strategy to create microporous architectures onto the filaments of PEEK lattice scaffold. Also, nanostructure and morphological tests of the PEEK-cHAp biocomposite were modeled and analyzed on the FDM-printed PEEK-cHAp biocomposite sample to evaluate its mechanical and thermal strengths as well as *in vitro* cytotoxicity via a scanning electron microscope (SEM). A technique was used innovatively to create and investigate the porous nanostructure of the PEEK with controlled pore size and distribution to promote cell penetration and biological integration of the PEEK-cHAp into the tissue. *In vivo* tests demonstrated that the surface-treated micropores facilitated the adhesion of newly regenerated soft tissues to form tight implant-tissue interfacial bonding between the cHAp and PEEK. The results of the cell culture depicted that PEEK/HAp exhibited better cell proliferation attachment spreading and higher alkaline phosphatase activity than PEEK alone. Apatite islands formed on the PEEK/HAp composite after immersion in simulated body fluid of Dulbecco's Modified Eagle Medium (DMEM) for 14 days and grew continuously with more or extended periods. The microstructure treatment of the crystallinity of PEEK was comparatively and significantly different from the PEEK-cHAp sample, indicating a better treatment of PEEK/cHAp. The *in vitro* results obtained from the PEEK-cHAp biocomposite material showed its biodegradability and performance suitability for bone implants. This study has potential applications in the field of biomedical engineering to strengthen the conceptual knowledge of FDM and medical implants fabricated from PEEK-cHAp biocomposite materials.

Keywords: 3D printing, PEEK-cHAp biocomposite, Nanostructure, Bone implant, Composite morphing.

Introduction

The recent development of medical devices through the advent of polyetheretherketone (PEEK), structurally represented as (-C_6H_4-OC_6H_4-O-C_6H_4-CO-)n, has seen an increasing trend due to its desirable mechanical properties. These properties include but are not limited to, excellent cellular biocompatibility, strength and an appropriate elastic modulus [1]. Moreover, PEEK has been used in a variety of clinical applications that include vertebral and cranial reconstruction [2]. Also, the addition of nano silicate crystals to PEEK increased the binding, number and progression of PEEK-associated cells. PEEK coated with titanium (Ti) and calcium hydroxyapatite (cHAp), with a structural formula of $Ca_{10}(PO_4)_6(OH)_2$, showed that the bone and the contact rate of artificial tooth roots were higher than for a pure PEEK transplantation [3].

Analysis of strategies to increase the biological activity of PEEK has been investigated, where mixed injection, compression moldings and cold selective laser sintering (SLS) were used to produce PEEK-cHAp and beta-tricalcium phosphate (β-TCP) composite materials [4]. Functional PEEK-cHAp biometry has been produced by layering extrusion, which is suitable for the mass production of low-cost PEEK compounds and, more importantly, porosity was obtained within the immersion time by dissolving sodium chloride in the solvents [5]. SLS is a type of additive manufacturing (AM) technology that specializes in the production of PEEK parts with highly complex structures, allowing more complex design freedom [6, 7]. The first bioactive PEEK treatment method failed to control the bioactive phase of the PEEK matrix, which made the PEEK and the bioactive materials dependent on the filament combination. The shape and density of these particles help to prevent mixing, which is generally useful and consistent [8]. In this present study, a new technique has been proposed to control conductivity. This technology combines the proposed processes of extrusion and AM, based on extrusion production, with the associated new possibilities for the production of biologically productive pore structures, the supply of PEEK and the efficiency of biological compounds. Designers have been able to precisely control the phase distribution of the bioactive substances in the PEEK matrix and adjust the quality, biological and mechanical properties of the final mixture. Also, the biocidal phase and the PEEK matrix are interconnected, which is superior to the traditional microstructure design [9]. This method can be used for several physiological agents, such as Bioglass and β-TCP, among others. It can be used at different speeds due to its biodegradation. 3D channels have been connected to increase growth rate and spread. The network was related to the physiological activity of body absorption. Thus, the bone structure fixed in the PEEK was performed *in vivo*, which significantly increased the fixation of the implantation compared to general techniques [10].

Moreover, PEEK and its compounds remain relevant in clinical dentistry due to their aesthetics and incredible biomechanical properties [11]. Studies have suggested that the PEEK material has a lesser resistance to stress than more traditionally used dental materials, such as titanium [12]. Given the physical properties of bones, PEEK can be used in many areas of dentistry. However, increasing the biological activity of PEEK dental implants without compromising their mechanical properties is a great challenge [13, 14]. Also, PEEK is not toxic, mutagenic, or causes significant inflammation [15]. Also, the production of teeth and face devices for the jaw, although small, is a challenging task and must be adequately understood to apply the available technologies fully. 3D printers, which are compatible with computer-aided design/manufacturing (CAD/CAM), give a significant advantage because their use has a negligible effect on the mechanical properties of PEEK and can otherwise retain the desired specifications [16]. Therefore, it is an effective way of 3D printing PEEK to develop dental implants, prostheses and crowns. Also, crowns and fixed partial dentures (FPDs) are usually made of ceramic or composite resin, and the application of PEEK is still not sufficiently utilized [17]. A hybrid production route comprising fused deposition modeling (FDM) and silicone molding processes has been used. First, a unique template was sterilized and then intraoperatively was used to create the associated implant [18].

Recently, there has been an increased development of medical devices using PEEK materials. This is due to their suitable mechanical properties as well as the modulus of elasticity of the cortex, leading to increased biological compatibility with cells and bones. Several manufacturing procedures, such as injection molding, particle leaching, laser extrusion and SLS have been used to produce porous PEEK for biomedical applications. Although many studies have been conducted to provide porous additives from porous structures using a variety of materials. There are still few detailed reports on AM-extrusion of poor-quality PEEK parts and weak mechanical properties, such as bending and separation [17-19].

Furthermore, PEEK is always physically and chemically stable and needs modification using either physical or chemical processes [19]. PEEK is biologically ineffective and often causes inadequate fixation of the implants. Their looseness, in severe cases, often results in defective areas [20]. For any potentially biodegradable application, mainly

orthopedic, the replacement should have reasonably good cytological compatibility [21]. For their injection, the enhancement of bioactive materials is often desirable to meet these requirements. It has been reported that the sulfonation of PEEK occurred through immersion in concentrated sulfuric acid, causing geometric deterioration [22]. It has been demonstrated that the proliferation of rat osteoblasts, in terms of the size and number of binding adhesion plaques involved in cell proliferation, were comparable in PEEK, titanium, and chromium-cobalt-molybdenum alloy [23]. However, contradictory results that questioned the interaction between PEEK and osteoblastic differentiation have also been reported [24]. For example, PEEK implants formed bone *in vitro* that was comparable to that from coarse titanium [25].

Moving forward, it was reported that osteoblasts were less different in the case of PEEK than on titanium surfaces [25, 26]. As the titanium-PEEK compound allowed a better osteoblastic differentiation than the PEEK itself, a possible PEEK-Halo effect was present [27, 28]. In general, the results highlighted in biomedical devices with PEEK material are paradoxical. According to the literature, it is difficult to understand the reality of the *in vivo* and *in vitro* properties of the PEEK material. Therefore, the successful extrusion of a PEEK structure through an extrusion system was coordinated to elucidate critical challenges, with an in-depth discussion of process parameters that are thus given in this present work. Many mechanical properties obtained from the previous studies or literature have established that platform injectors and ambient air temperatures are the most critical thermal parameters for printing. Therefore, the mechanics, as well as the analysis of printed samples, were at the maximum temperature limit.

Considering orthopedic implants, PEEK is the most widely used biomedical device in the world. The main reason for the customization of the popularity of printing, surgeons, bones, and defective 3D members is to help understand and change the specific anatomical model of the patient that allows for the creation of products [29, 30]. Also, problems relating to the spine, knee, elbow, hip fractures, and severe orthopedic issues related to 3D printing and high-performance materials can be quickly dealt with [31]. How to perform preoperative planning using a printed model to minimize both the time required for a patient's operation and blood loss has been investigated [32]. Another researcher has attempted to clearly define what 3D printing technologies would benefit orthopedic surgery [33]. The history of implantable PEEK is not new since it was introduced in 1999 by *In Vivo* Biomaterial Solutions, London, UK. Fig. 1 shows the processes of enhancing the mechanical performance of PEEK implants.

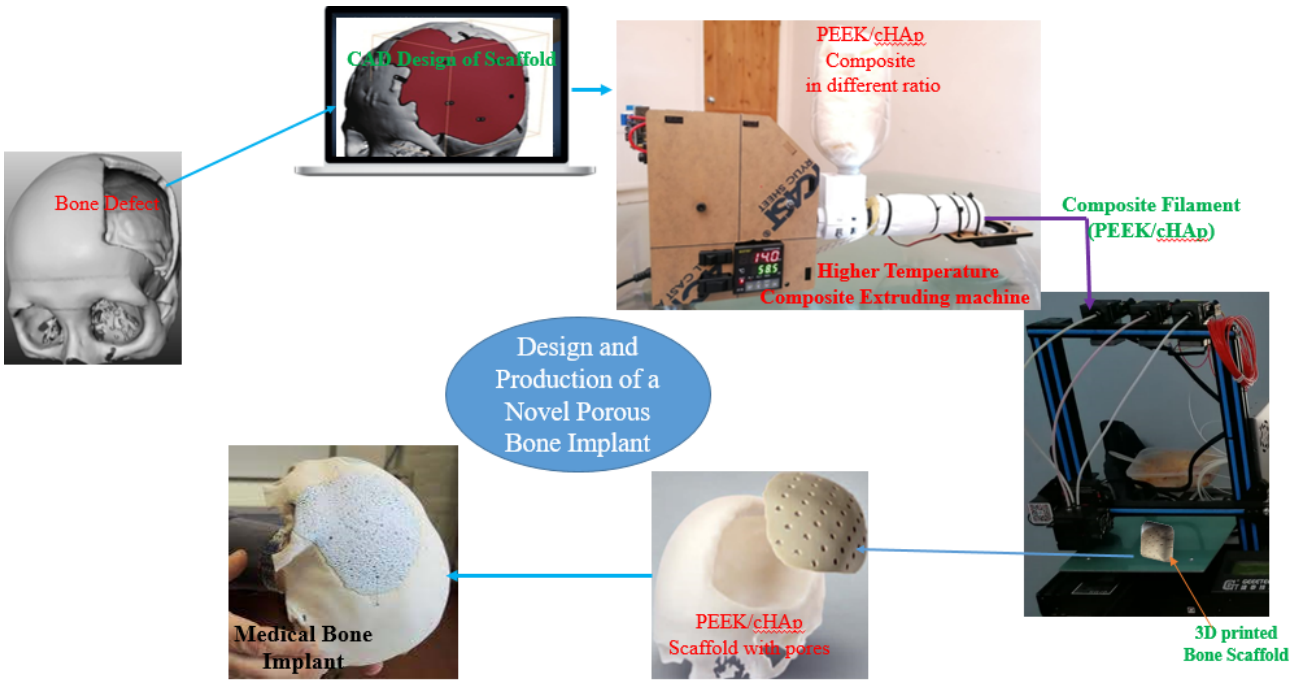

Fig. 1 A summary of the schematic filament production of composite via high temperature extruding machine and 3D printing of PEEK composite in biomedical scaffold for bone implant

Also, processed and printed PEEK implants have already been used in humans and animals without major complications [33-35]. However, printed PEEK implants have not been investigated in detail, using SLS and FDM parts with sintered PEEK grade sintering the acceptable section of the bone porosity, excellent mechanical performance, which has chemical stability and biocompatibility [34-36]. In particular, centrifugation coating, plasma gas treatment, and electron beam deposition of plasma or plasma immersion of cHAp ions have been employed to further improve the bioactivity characteristics. It is possible to use numerous approaches, as reported [37, 38]. An average pore size of 279.9 ± 31.6 µm, support lagoon of 186.8 ± 55.5 lm, a surface that has an interconnection porosity of 67.3 ± 3.1% and 99.9 ± 0.1%, and porous PEEK material have been reported [38, 39]. The monotonic tensile tests showed that the strength of the material was 73.9% when compared with the molded PEEK. Also, a model of osseointegration in a mouse showed a significant bone formation within the pore layers at 6 and 12 weeks, using micro-computed tomography technology and histological evaluation. The overall results indicated that the material produced an improvement in ossification, maintaining structural integrity. Therefore, the PEEK material can be used as a support surface in arthroplasty. It can be processed using 3D printers to obtain a customized implant geometry. This site or company-based processing can be used to create a bearing surface that can meet the current implant standards established by the American Society for Testing and Materials (ASTM) and, more importantly, by the Food and Drug Administration (FDA) department. The bacterial resistance of the PEEK implant results from the use of nanocolumns with random capillary distances was compared with their copolymers. After five days, the PEEK prevented 37% more staphylococcus.

Therefore, to benefit from the excellent mechanical behavior, good processability, and remarkable thermal stability of PEEK biomaterial, it was combined with the main component of bone (cHAp) to produce an attractive, efficient, and optimized PEEK-cHAp scaffold biocomposite for bone implant applications, using an innovative combination of the AM/3D printing and FDM techniques, as the main objectives of this study.

Materials and method

The medical PEEK used in this study was obtained in two ways; PEEK-OPTIMA ™ LT1, developed at a stretched shaft diameter of 25 mm and an experimental filament diameter of 1.75 mm, according to the described procedure [40-42]. The mechanical properties of the PEEK filament used in this experimental investigation is present in used Table 1. LT1 is the most commonly used quality of PEEK for implant applications. The PEEK material for implant application was an injection molding medical-grade OPTIMA LT1 resin. It was obtained from Invibio Ltd. and is similar to its industrial-grade 450 G from Victrex Plc. It has a melting index of 3.4, a molecular weight of 115,000.23 amu, with a glass transition temperature of nearly 145 °C, a melting temperature of approximately 343°C, and a crystallization peak of 160 °C. JHS Biomaterials supplied a medical-grade HAp powder with a particle size of 200 mesh. The lumbar spine formulation used was developed according to the report of the ASTM collaborative studies [43-45]. The cache stereolithography (STL) file was created from a 3D model developed using the commercially available SolidWorks 2019 software package. Samples were cut, and commercially available 3D simplification software was used to generate the code numerically. Six cages were printed with several heating leaks. To prevent the collapse of the horizontal hub poles during printing, 3mm temporary support structures were formed on both sides of the cage. Also, edges were added to the cage to increase adhesion between the main object and the stopper. These support structures were removed from the cage after printing and before mechanical or physical property tests were conducted on the printed sample, using the relevant International

Organization for Standardization (ISO) standards, printing/process parameters, infill patterns and values presented in Tables 1-2.

The desired geometric shape of the final complex object was created under the control of a computer. The extrusion temperature was set at 380-410 ºC, and the printing speed was 40 mm/sec. The bead width of each print line was 0.4 mm, and the layer thickness was 0.2 mm (Tables 1 and 2). Also, the PEEK filler, which was a 3D printing material in this document, was reprocessed from pellets and 5% carbon fiber with a length of 80-150 microns and a diameter of 7µm was chosen as a backup.

Table 1 Technical specifications and printing parameters of the FDM for PEEK/cHAp

Parameters	Technical Specifications
Nozzle diameter	0.4 mm
Bed width	210 mm
Layer thickness	0.2 mm
Printing speed	45 mm/s
Raster angle	Longest edge
Ambient temperature	30ºC
Chamber Temperature	90ºC
Bult Plate temperature	110-160ºC
Nozzle temperature	350-410ºC

Table 2 Printing settings for fused deposition modeling

Extruder	Parameter	Infill	Value
Nozzle diameter (mm)	0.4	Internal fill pattern	Rectilinear
Extrusion multiplier	0.78	External fill pattern	Rectilinear
Retraction distance (mm)	0.49	Interior fill percentage	100%
Retraction Speed (mm)	1750	Outline overlap	50%
Layer		Infill extrusion width	90%
1st layer height (mm)	0.1	Minimum infill length (mm)	5
Top solid layer	3	Support	---
Bottom solid layer	3	Support infill percentage	30%
Outline shells	3	Print support layers	1
1st layer height	170%	Bed temperature	90ºC
1st layer width	95%	Nozzle temperature	390-445ºC
1st layer speed	30%	Z-axis movement speed (mm/min)	1000
Additions (skirt/brim)		Filament diameter (mm)	1.75
Skirt layers	1	---	---
Skirt offset from part (mm)	0	---	---
Skirt outlines	15%	---	---

Characterization and microstructure analysis

The software enabled the analysis of melt pool-scale phenomena for full-size components and provided detailed thermal history and microstructure information. It allowed single-bead simulations to be run for quick evaluation of melt pool sizes and shapes. It also regulated the porosity in part, due to deficiencies in the fusion of selected sets of procedure parameters. The microstructure and topology optimization of the PEEK-HAp biocomposite was carried out. The software window for the nano-microstructural analysis of the materials is shown in Fig. 2. Multiple static loads combined with optimized natural frequencies modal analysis were considered, which satisfied the requirements for minimum material thickness. The rules around the feature direction for machining operations were observed, for example, having scope for both cyclic and planar symmetries, which helped to validate results promptly. The tools within Digital Surface (Mountain 8 Premium) Mechanical for topology optimization were fast, easy to use, and were included with all the current licenses of the ANSYS Mechanical product family.

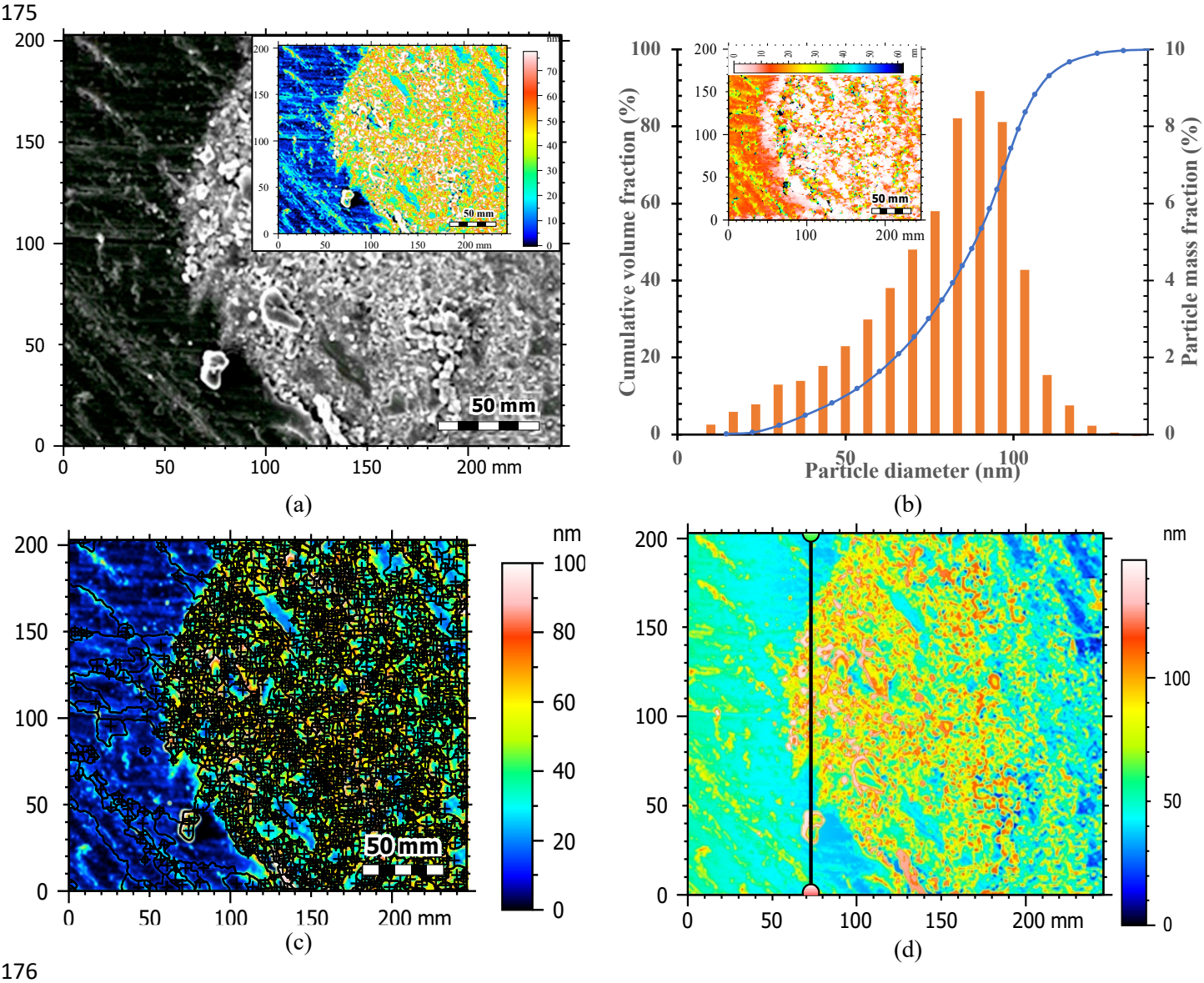

Fig. 2 SEM morphology and analysis platform of the PEEK-HAp, depicting (a) MG-63 cell attachment and proliferation scaffolds, (b) the surface Karhunen-Loeve (K-L) transformed, (c) surface conversion of the luminance of particle analysis, and (d) waviness filter of Daubechies

Cell Culture Medium

The cells were cultured in DMEM culture media pouch, low glucose, 5/Pack (Hyclone, Thermo, USA) supplemented with 10% fetal bovine serum, 1% penicillin/streptomycin and 1% GlutaMAX in 75 cm^3 sterile cell culture flasks. The medium is a basal medium for growing various types of mammalian cells. DMEM gives a fourfold enhancement of amino acids and vitamins in the original Eagle's medium. The economical DMEM powder is easy to transport and store, having low glucose levels of 1g/L with little or no $NaHCO_3$ and Phenol Red of L-glutamine without Sodium Pyruvate. The cells were cultured at 37 °C in a humidified atmosphere with 5% CO_2. The culture medium was replaced every day. The formulation was 9.9 g of powder for 1 L of DMEM medium with sodium bicarbonate [32]. A volumetric flask was filled with distilled water of 800ml and a complete DMEM of 13.10gram was added and stirred in a glass jar. Sodium bicarbonate of 0.6g and the remaining 200ml of distilled water was added to make up of 1liter of distilled water and a vacuum filtration media was done. A Fetal Bovine Serum of 100ml with 1% of the total media of antibiotics was added.

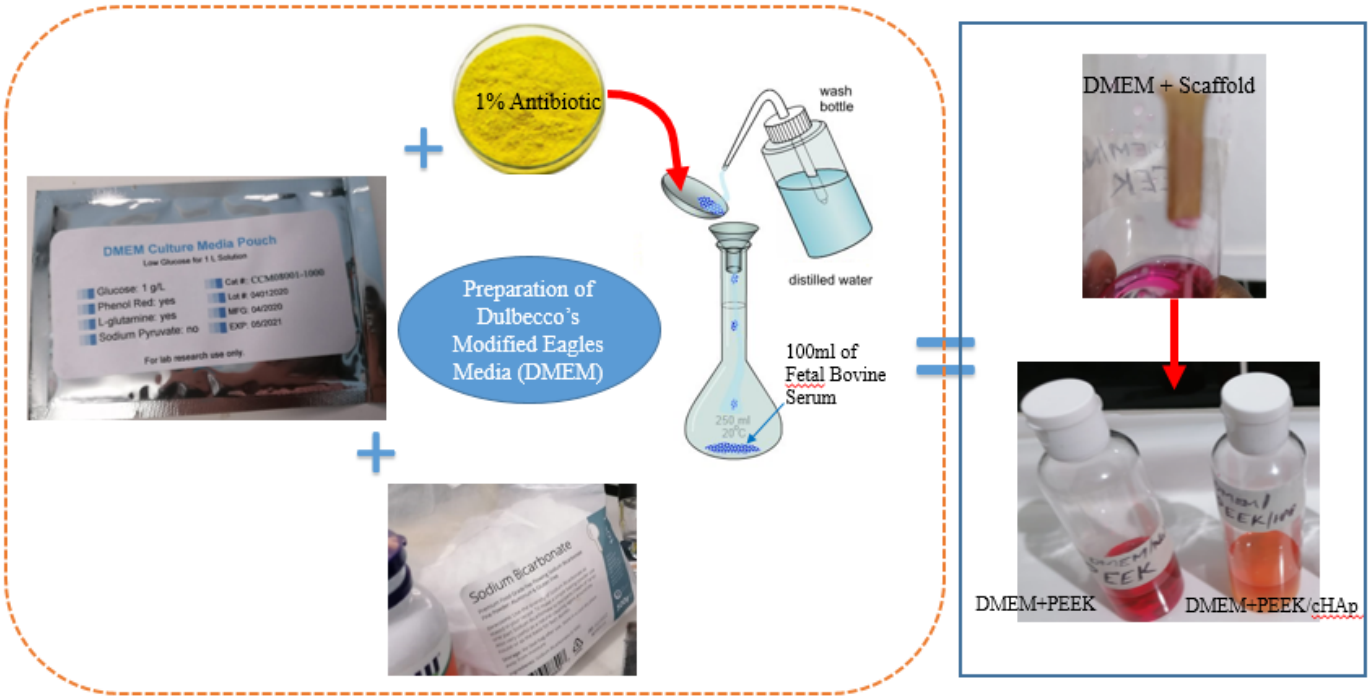

Fig. 3 The experimental set up for the DMEM culture media of low glucose

Mechanical and microstructural analysis

3D mesh samples for microstructure analysis were cut with the aid of a diamond cutting tool. A morphological study of the printed 3D parts and the porous delineation was conducted, using optical and scanning electron microscopies. Also, the printed PEEK scaffold was described in terms of porosity and mechanical properties. Porosity is measured by the correlation, geometry and density of PEEK material following the ASTM F 2450-04 standard, using Eq. (1).

$$Porosity\ (\%) = \frac{\left(V_t - \frac{m}{\rho}\right)}{V_t}\ x\ 100 \quad (1)$$

Where V_t represents the total volume used by the pore network. This was determined by the length, width and height measurements. The density, ρ, of the material was 1.30 g/cm3 for the Victrex® PEEK 450G. Mass, *m* of the sample was measured with a Mettler AE240 weighted microphone. According to the standard compression test method specified by ASTM D695-02a, stress-strain reactions were investigated in the printed porous closed-cell samples, using the following dimensions: diameter of 12.5 mm, the height of 25 mm, porosity of 600 80 m, support height of 200 100 m and pore size of 450%. A porous hot plate with a maximum pore temperature of 4%, an average porosity of 38% at 100 °C, and an ambient temperature of 80 °C was used. The samples were tested at a tensile rate of 10^{-3} s^{-1}, using an Instron 8032 testing machine. 100kN load cells and Instron test data in smart 6200 strain software were used. Solid samples of PEEK-OPTIMA LT1 0% porosity were analyzed to compare them with a 38% sample. Three porosity samples were tested for repeatability. For each group, the flexible structure of the PEEK during the compression of the sample was deformed for large species, and all the species mentioned in this study were direct. Compressive strength is defined as the pressure at the first linear limit at which the species deviates from a straight line. Performance limitations refer to the stress associated with compressive force.

Daimler lead twist analysis

3D printed PEEK scaffolds with different fill sizes were used for the FDM of the scaffold. They were used in the extrusion process to produce PEEK-HAp compounds with a static load and to prevent air from entering the composite mold. It was

prepared from a 0.5 mm vent hole in the bottom surface with steel and a 25 mm bore. The ideal formation temperature was 400 °C, and a 10 x 10 x 3 mm^3 outer structure was molded with a pressure of about 0.39 MPa and was tested. The mold was tested with different sizes of filler/porous HAp. The static charging method included a mold heated to 250 °C, and the load and pressure continued to increase till the temperature reach 400 °C. Heat and weight were maintained for 20 minutes. The PEEK crystallized and hardened after the mold was cooled under pressure. The individual HAp fibers of the first HAp platform and the PEEK lines that penetrated the absorbed PEEK were evaluated to determine their surface hardness values. The average surface hardness values of each of the five examined or inspected areas were recorded. Fig. 4 shows the values of the parameters for the PEEK-HAp. The Daimler lead twist had a diameter of 40 µm, after setting the period length, theoretical supply cross-section, and per turn of contact length in percent to be neutral. The evaluation length was set to be -1 µm at a maximum wavelength of 0.4 µm, as depicted in Fig. 2.

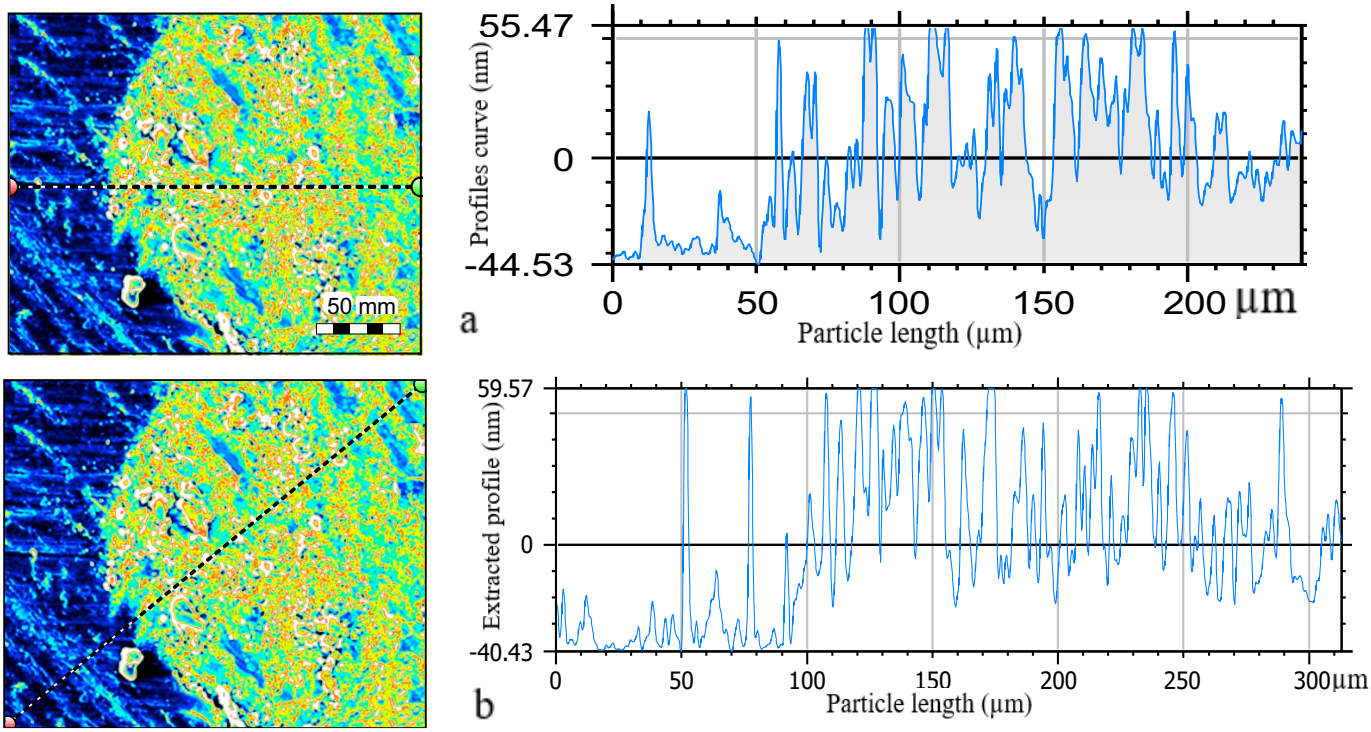

Fig. 4 Parameter values of the PEEK-HAp composite, showing (a) curve extracted profile of length 144-159 mm and (b) filtered extracted waviness profile of Gaussian filter settings, with a cut-off of 2.50 mm

The sample was set under ISO 4287 spacing parameters of roughness profile (RSm) at a 1.29 mm Gaussian filter of 0.8 mm at an amendment value (Rdq) of 7.86 x 10^{-5} degree. The peak parameter roughness profile (RPC) of 0.126 mm^{-1} at a tolerance of +/-0.5 nm on the same Gaussian filter value was set. The material ratio parameters of the first profile (Pmr) were at 100% under the highest peak Pmr of 1000 nm to 3000 nm, as presented in Table 3.

Table 3 Principles and characteristics are influencing parameter setting of the converted luminance of the tissue engineering for a scaffold in the 3D printing of PEEK-HAp

Parameters	**PEEK-cHAp**	**Parameters**	**PEEK-cHAp**
ISO 25178: Height parameters		**Feature parameters**	
Root-mean-square height (Sq.)	20.1 nm	The density of peaks (Spd)	0.0173 mm^{-2}
Skewness (Ssk)	1.93	The arithmetic mean peak curvature (Sq)	8.74 x 10^{-5} mm^{-1}
Kurtosis (Sku)	7.13	Ten-point height (S10z)	39.8 nm

Maximum peak height (Sp)	76.5 nm	Five-point peak height (S5p)	53.7 nm
Maximum pit height (Sv)	23.5 nm	Five-point pit height (S5v)	-13.9 nm
Maximum height (Sz)	100 nm	The density of peaks (Spd)	0.0173 mm^{-2}
The arithmetic mean height (Sa)	14.1 nm		
Functional parameters		**ASME B46.1: 3D parameters**	
Areal material ratio (Smr)	100%	Mean height in absolute (Sean)	5.99 x 10^{7} nm
Inverse areal material ratio (Smc)	23.7 nm	Developed area (Sdar)	1.9 x 10^{4} mm^{2}
Extreme peak height (Sxp)	17.3 nm	Projected area (Spar)	1.9 x 10^{4} mm^{2}
Spatial parameters of s = 0.2		**Hybrid parameters**	
Autocorrelation length (Sal)	20.6 nm	Root-mean-square gradient (Sdq)	1.97 x 10^{-5}
Texture-aspect ratio (Str)	0.425	Developed interfacial area ratio (Sdr)	1.96 x 10^{-8}%
Texture direction (Std)	92.3°		
Volumetric functional parameters of p = 10%, q = 80%		**Stratified surfaces parameters of Gaussian filter, 0.8 mm**	
Material volume (Vm)	2.5 x 10^{-6} mm^3/mm^2	Core roughness depth (Sk)	0.847 nm
Void volume (Vv)	2.62 x 10^{-5} mm^3/mm^2	Reduced summit height (Spk)	0.87 nm
Peak material volume (Vmp)	2.5 x 10^{-6} mm^3/mm^2	Reduced valley depth (Svk)	1.07 nm
Core material volume (Vmc)	1.3 x 10^{-5} mm^3/mm^2	Upper bearing area (Smr1)	14.1%
Core void volume (Vvc)	2.55 x 10^{-5} mm^3/mm^2	Lower bearing area (Smr2)	86.2%
Pit void volume (Vvv)	7.34 x 10^{-7} mm^3/mm^2	Material ratio at Plateau-to-valley	95.8

Results and discussion

In vitro cytotoxicity

Central heat, PEEK head extrusion design, nozzle or high temperature and environmental management for continuous printing without clogging the degradation factor of the polymer were shown from the experiments. The plate has a sufficient consideration for the adhesion and reduction of the curvature of the printed part syringe design on the extruded base of the head, heat on PEEK did not achieve adequate control. The raw materials of the PEEK syringe were ejected into the needle, which prevented the thermal decomposition viscosity which help in the *in vitro* control. Also, the syringe system was based on the testing limits on the number of printed parts. An extrusion syringe was used as the three-level PEEK jetty print, since the heat buffer's preliminary results on glass, per temperature, changed during the printing process. In Fig. 5, many alkaline phosphatase staining spots were observed in the blue PEEK/cHAp compound, and these spots were always denser than the spots on the PEEK surfaces. The relative alkaline phosphatase activity of cells in the PEEK/cHAp compound was significantly higher on day 14 than in the PEEK, p = 0.005 is example of *in vitro samples* (Figs. 5a-f) similar to [53-55]. More prominent actin filaments that adjacent bound cells have been observed in PEEK/cHAp. Also, the cell nuclei in the PEEK/cHAp compound were denser than the cell nuclei on the PEEK surfaces.

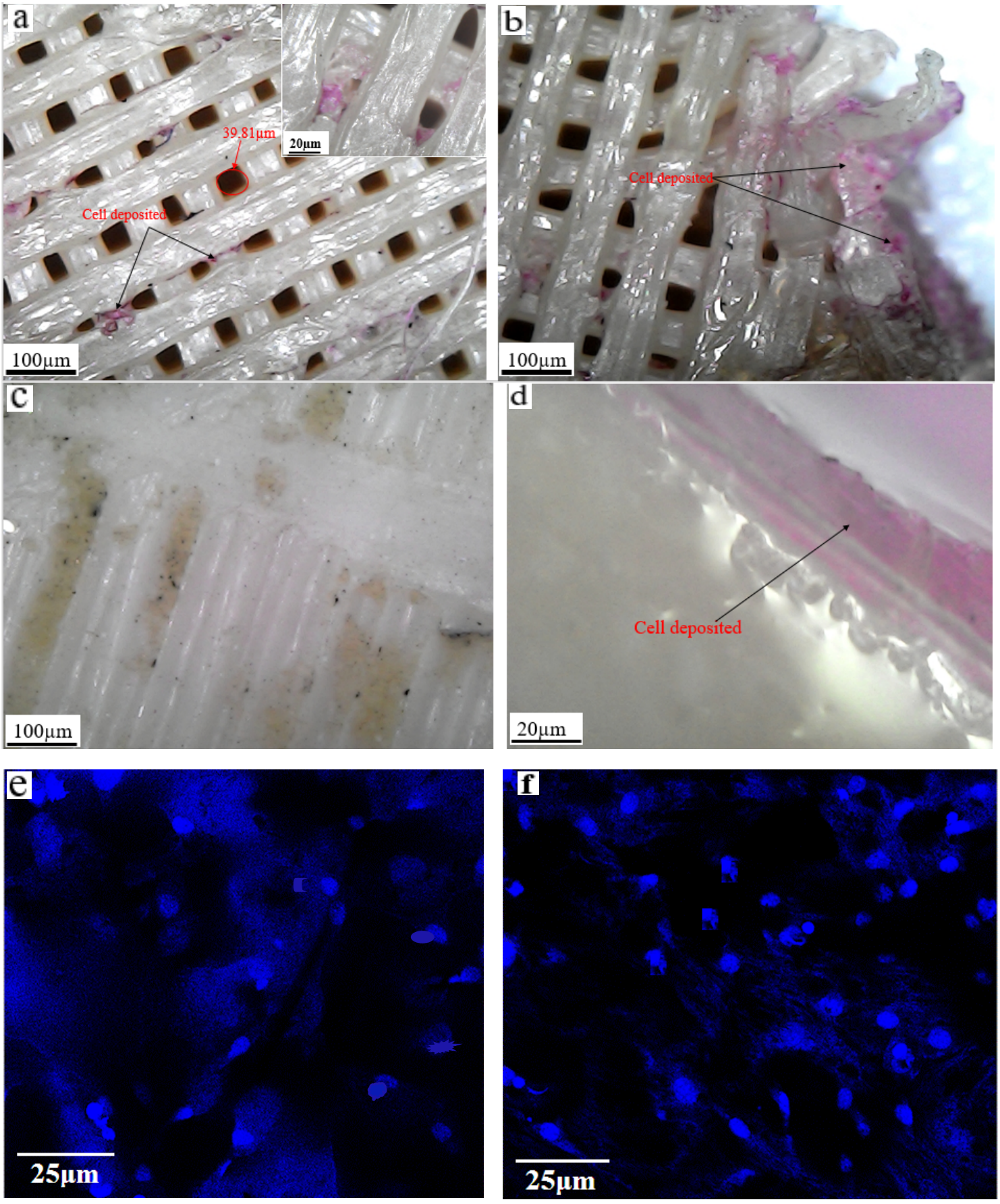

Fig. 5 The cells attached to FDM 3D printed PEEK composite sample surfaces after culture with pink colour (a) 100µm magnification of PEEK with 20 µm (b) 100µm magnification of fracture PEEK (c-d) spreading cell activity of cells when staining different material surfaces after days of PEEK/cHap with different magnification (e-f) filamentous action

of the cytoskeleton with SEM after incubation for days of morphology nuclei staining with 4, 6-diamidino-2-phenylindole 0.1 µg/mL in blue of PEEK and PEEK/cHAp

Mechanical test

The general charge displacement curve of composite samples with different cHAp content is shown in Fig. 6. It can be observed that the elongation decreased steadily with an increase in cHAp content, corresponding to the composite effect. Inorganic polymer nanocomposites of PEEK-cHAp showed a sticky and brittle failure behavior [54-57], depending on the amount of cHAp included in the PEEK composite matrix with a volume of up to 7.5% of cHAp. There is currently a plastic deformation phase before the mistake. In compounds with a cHAp content of more than 10%, they show the most fragile defects in the elastic region. However, the 40% tensile strength (45 ± 2.5 MPa) of the PEEK/cHAp composite is less than 50 MPa, which is not appropriate for cortical bones. When evaluating the elastic and elastic properties of PEEK/cHAp with different cHAp content, the 30% of cHAp content by weight was selected as the most suitable in terms of the effect on tensile strength, and in the modulus of elasticity of the PEEK/cHAp composite, which at 7 GPa represents the modulus of elasticity of the lower band. The 5% volume weight line represents the tensile strength of the bone-implant, which has a smaller part of the bone cortex of 5% volume PEEK/cHAp composite (Fig. 6).

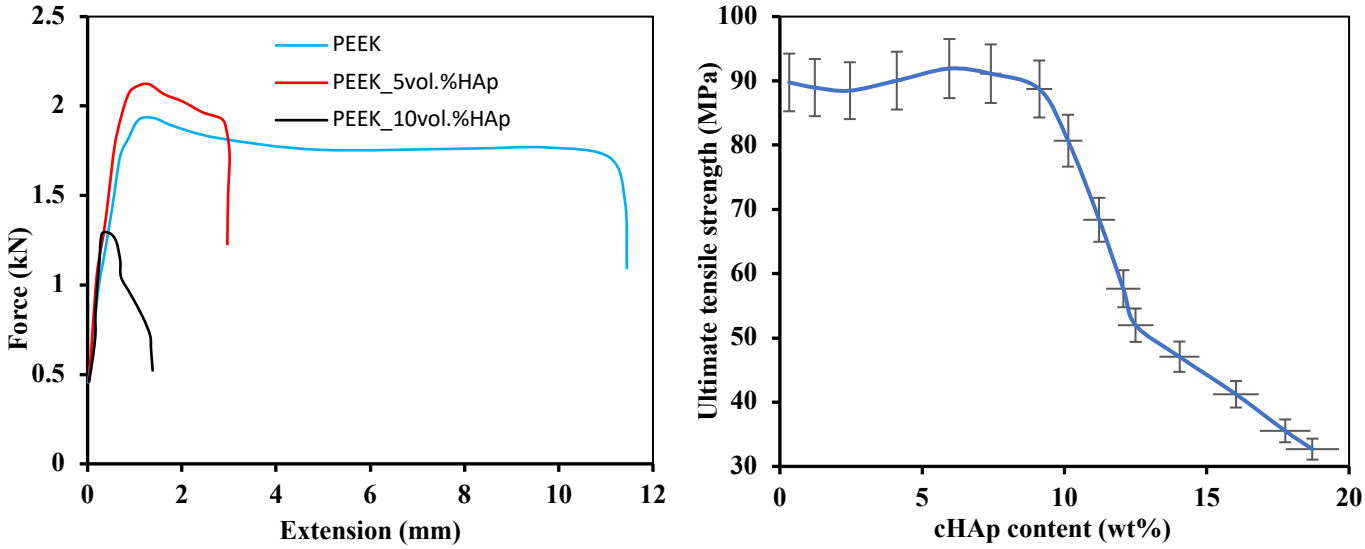

Fig. 6 (a) The force-extension curves of the PEEK–cHAp composite samples at different percentage volumes and (b) variations of the ultimate tensile strength (UTS) with percentage weight of the composite material of cHAp

The relationship between the UTS of the composite material and the nano-cHAp content, as observed in Fig. 6, was different from the PEEK/cHAp compound with medium cHAp loads, showing that addition of any amount of cHAp to PEEK reduced the tensile strength. On the other hand, the present study showed an increase in the tensile strength of the composite material with the content of the cHAp nanoparticles at given moment when the nanocomposites successfully synthesized with the PEEK to produce a good composite. Considering the microstructure of compounds with a 5% volume of nano-cHAp, all the three pillars layer was irregular (Fig. 7), due to low temperature management in the PEEK syringe extruder. The threshold watershed detection method was obtained at 51.58 nm with 1336 nanoparticles, having a projected area of 37.48 µm². With this length-scale method, the equivalent diameter of 5.837µm possessed 200 points with a maximum domain scale of 246.1 µm. According to Fig. 7, the smooth-rough crossover (SRC) was obtained at 4.592 µm with a fractal complexity (Lsfc) of 8.923 x 10^{-8}, a scale of maximum complexity (Smfc) of 1.675 µm, and a length-scale anisotropy (epLsar) of 1.8 µm, at 5°.

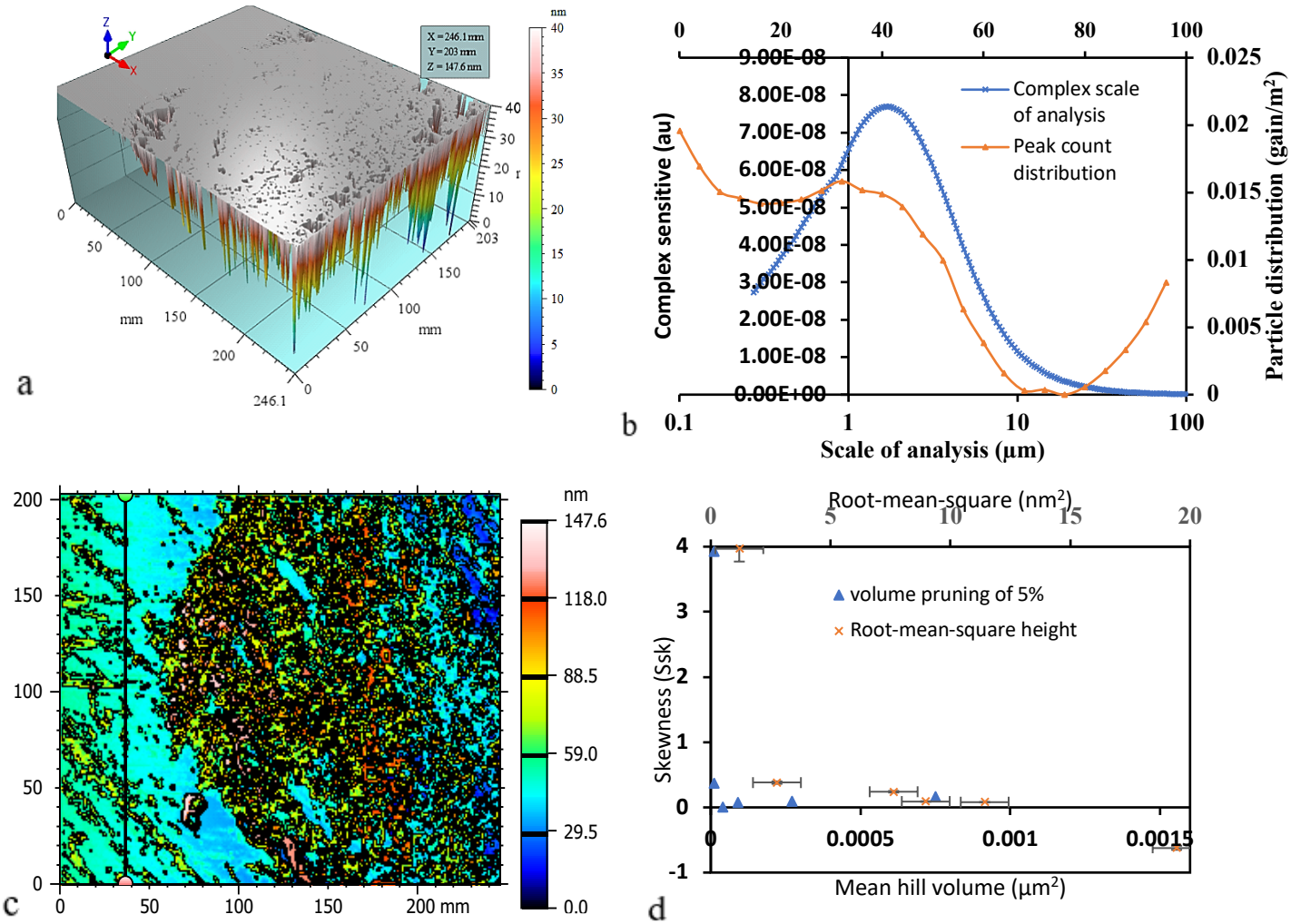

Fig. 7 Parameters of the PEEK-cHAp biocomposite, showing (a) 3D view of the wavelet filter of Daubechies of 10, (b) peak count distribution of compatibility complex sensitive microanalysis of particles, (c) nanoparticle segmentation with thresholds of -60.8 nm and 39.1 nm of 1336 number of nanoparticles and (d) skewness with a mean hill volume pruning of 5% scatter plot with a root-mean-square height of K-L transformed

Also, if the extrusion temperature were too high, the amount of material would reduce, or the molten plastic might not retain its shape after settling, resulting in fiber deformation and dimensional errors. On the other hand, if the temperature was not high enough to allow time to dissolve in the material thoroughly, this might cause nipple blockage. In particular, the fiber base has less time to completely absorb and dissipate the energy of the PEEK fiber, the extrusion head. The affected area was used when the affected heating zone was substantially smaller than the head. Depending on the gun, a low-temperature extrusion might also cause stratification because the material has insufficient energy to reach the previous contact. Also, there was a relationship between the temperature of the nozzle in the fiber, the system based on extrusion and the extrusion of the flow. For example, if a high flow rate was required to shorten the build time, a thick layer of the printing material must be used with little time to absorb the energy produced in the clogging nozzle. Therefore, the high temperature of the nozzle was necessary to prevent the nozzle from clogging at high flow rates. Table 4 shows the parameters of the resampled series in ISO 25178.

Table 4 Parameters of the resampled series in ISO 25178

Description	Mean	Std. Dev.	Sum	Range	Variance
Height parameters					

Root-mean-square height (nm)	9.32	4.07	55.9	13.2	16.6
Skewness	0.389	0.969	2.33	3.04	0.940
Kurtosis	8.29	9.46	49.8	27.4	89.5
Maximum peak height (nm)	48.3	12.6	290	34.1	160
Maximum pit height (nm)	46.7	12.9	280	31.7	167
Maximum height (nm)	95.0	24.4	570	61.7	596
Arithmetic mean height (nm)	7.14	3.96	42.8	12.8	15.7
	Functional parameters				
Areal material ratio (%)	100	0.00	600	0.00	0.00
Inverse areal material ratio (nm)	10.7	4.57	64.0	15.4	20.9
Extreme peak height (nm)	19.2	9.34	115	30.4	87.3
	Spatial parameters				
Autocorrelation length (nm)	5.12	8.91	30.7	24.8	79.5

Surface imaging characterization

The average pore size of all cohorts printed ranged from 81µm to 135µm, the correlation between printing speed and average pore size (PCC = 0.37; p = 0.08) was obtained. The average pore size was zero, and it was significantly lower than that of all groups at p = 0.01 for the whole test. The SEM images at 3000 mm/min were used to observe the cohort. Cracks were found in the print layer, which was attributed to weaknesses. The morphology of the fracture surface was the same for all groups printed under the same loading conditions; it started in parallel with the layers, then changed direction and was placed perpendicular to the layers. Fig. 8 shows the energy dispersive spectroscopy (EDS) phase map collected with these characterized microstructures. The Carbon Kα1 phase (in red) can be easily identified, as it contrasts with the other phase that has green microstructures of oxygen Kα1, as presented in Figs. 8(a) and (b), respectively

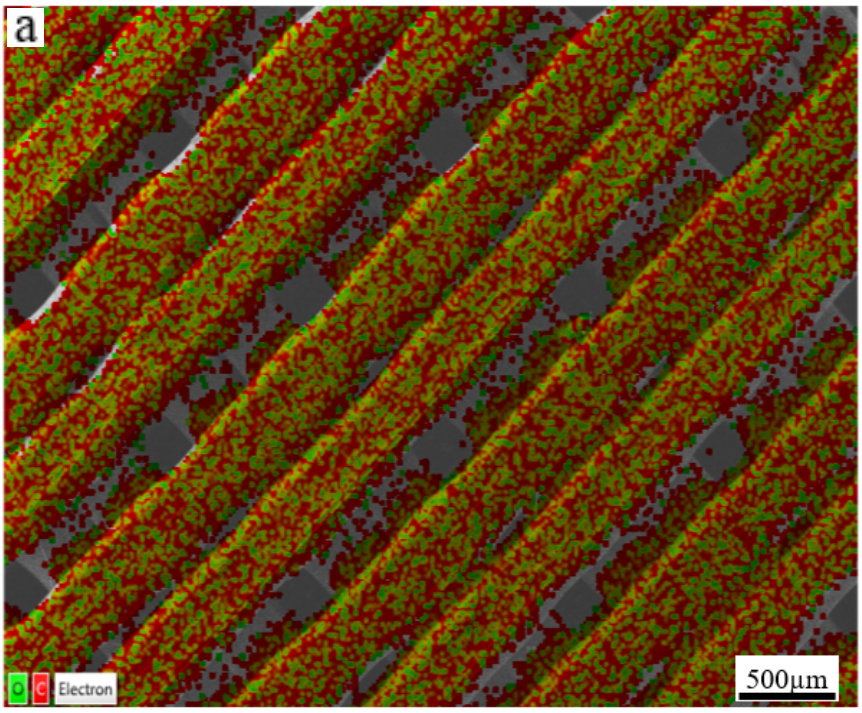

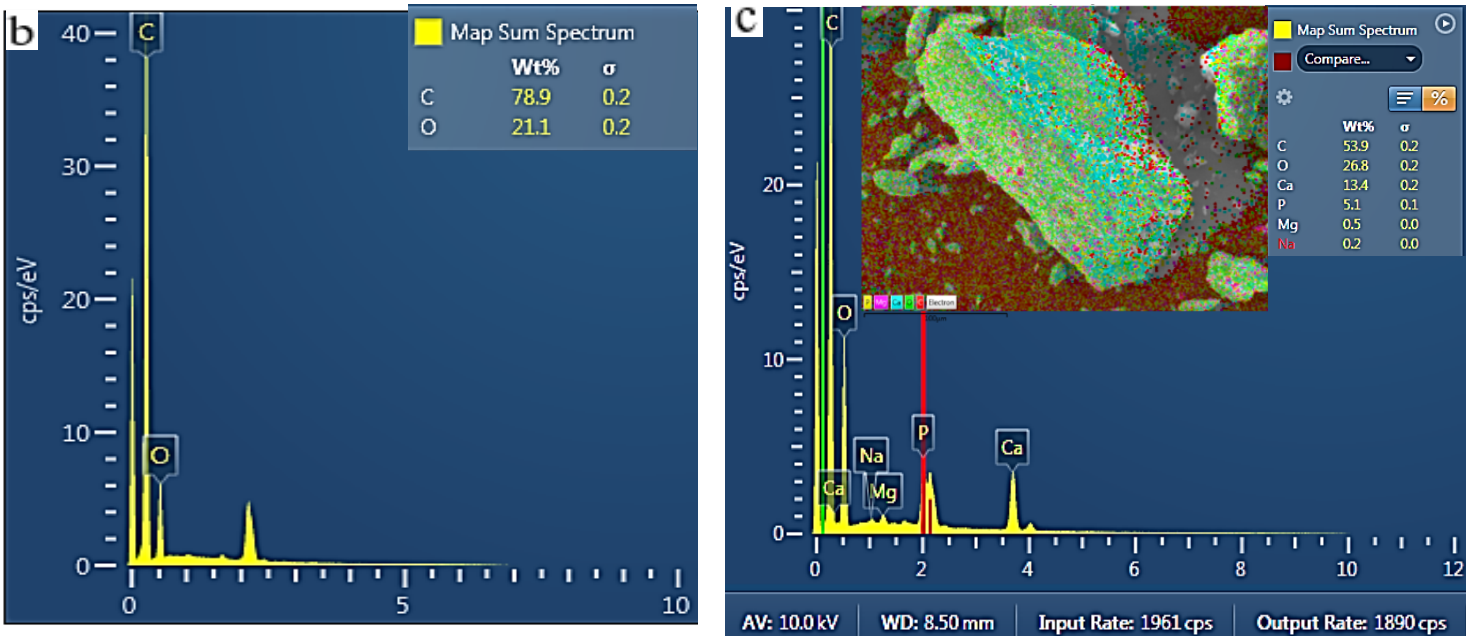

Fig. 8 Characterization of microstructures, showing the elemental mapping for (a) microstructure elemental mapping for PEEK in 2 layers of EDS of Carbon 78.9wt% and 21.1wt% of oxygen (b) the EDS spectrum for PEEK and (c) EDS for cHAp at 100 µm

The parameter for the PEEK-cHAp, the 3D view of surface K-L transformed, fractal compatibility analysis of the enclosed scale of K-L transformed, the frequency spectrum of K-L transformed and average power spectrum density of K-L transformed are shown in Figs. 9(a)-(d), respectively. The frequency spectrum parameter value has a unity wavelength of 0.5348 µm with an angle of -44.42°, and a frequency magnitude of -45.6 dBc with a phase value of -118.5°. According to Fig. 9, the morphological envelopes parameter value has a fractal dimension of 2.393 with a slope of 0.6073 and an R^2 value of 0.9975.

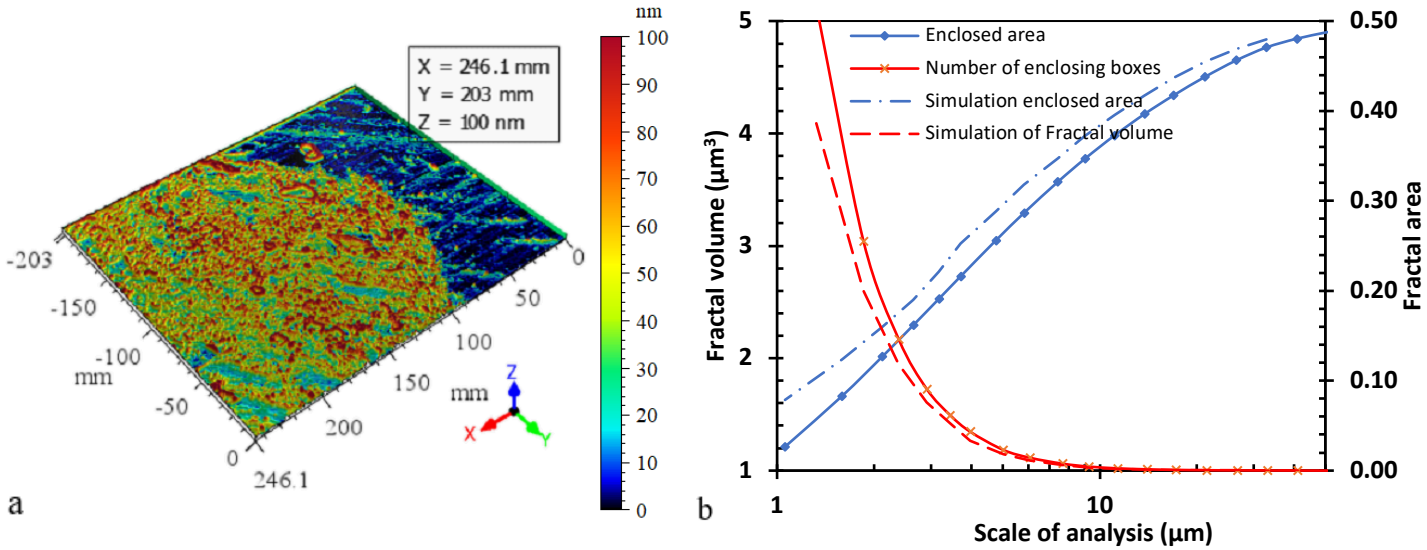

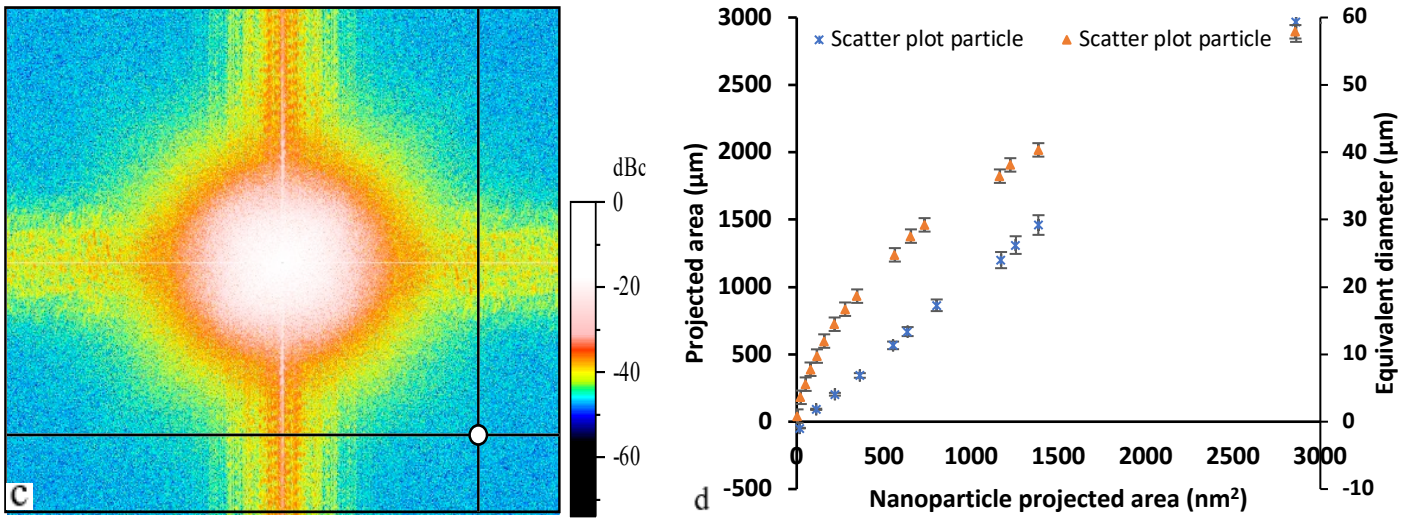

Fig. 9 Parameter values for the PEEK-HAp, showing (a) 3D view of surface K-L transformed obtained through the profilometry technique, (b) fractal compatibility analysis of the enclosed scale of K-L transformed, (c) frequency spectrum of K-L transformed, and (d) scatter plot of nanoparticle microanalysis at a projected area of K-L transformed

Nanostructure crystallinity of PEEK-HAp biocomposite

PEEK can limit the use of biocomposite structures as it increases the risk of structural failure. The evisceration of 3D-PEEK implants was examined using microscopic observations and porosity measurements. Samples with a fill rate of 100 and 80% have porosities of 14 and 31%, respectively. The porosity of 14% was obtained with a fill rate of 100%, mainly due to the formation of air spaces between fibers. Ground accumulation of different types of airbags was typically produced, because of the natural limitations of this process, which created space between layers. Also, the geometry of the fibers restricted the filling of the materials in each segment, thus creating unwanted gaps between the circumferences of the sheets and the loading fibers. These air channels tended to form in the first impression, where the workpiece was attached to the base material. Air winds, high operating temperatures and small bubbles were stored in the extruder to collect the bubbles in the filament material for the first time. All these defects contributed to the PEEK components formed by the extrusion technique. 3D printing with the most durable material and a nozzle temperature of 420 °C under the trade Ultem 9085/Stratasys FDM commercial machine was used for the targeted applications. The parameters of the PEEK-HAp biocomposite included the roughness of the wavelet filter with a Daubechies of 10, having a scatter compatibility control chart of height motifs analysis, and the histogram of compactness from the study of volume islands was 33 point, as shown in Fig. 10. The wavelength of the composite was obtained at 30.73 µm, with an amplitude of 5.892 nm, having a dominant wavelength of 24.93 µm and a maximum amplitude of 12.50 nm of the root-mean-square gradient (Sdq), as shown in Fig. 10.

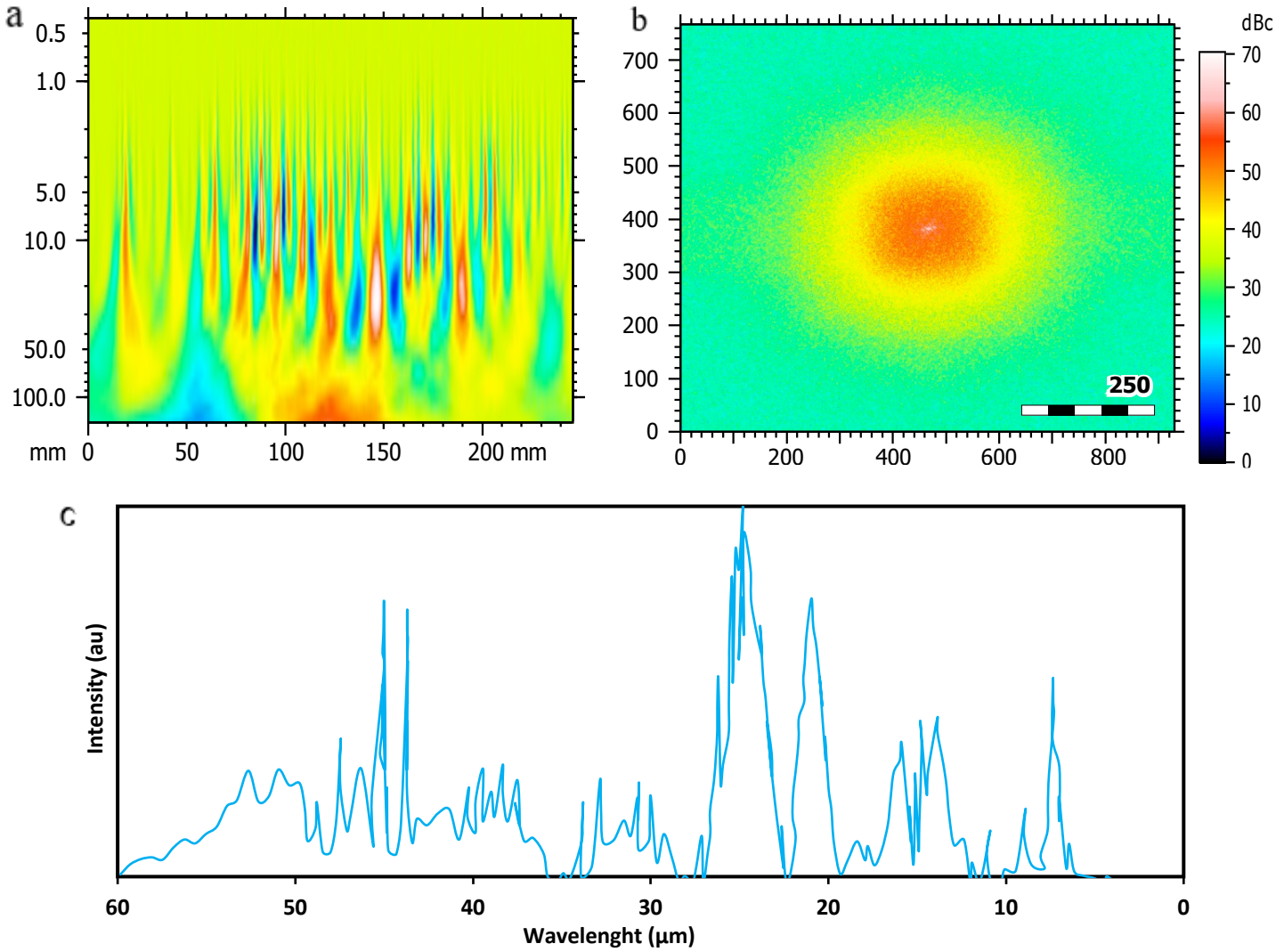

Fig. 10 Parameters for the PEEK-HAp biocomposite, depicting (a) continuous wavelength decomposition roughness of wavelet filter of Daubechies of 10, (b) scatter compatibility of the studied surface-generated fast Fourier transform (FFT) spectrum and (c) average power spectrum density motifs X-ray diffraction (XRD) pattern analysis

Moreover, the PEEK with a porosity of 31% exhibited UTS of 49.22 MPa and a failure of 0.31. Therefore, the inclusion of 17% porosity caused by an increase from 14 to 31% in the 3D printed samples was appropriate and produced reductions in UTS by 35% and 13%, respectively, under the failure to fail concept. It should be noted that the UTS of the printed porous PEEK samples was compared with that of PEEK-HAp compounds with a similar cHAp content. The significant difference in the stress-strain curve of the PEEK components and the 3D printed/injection molded components can be attributed to different fracture mechanisms. In contrast, samples processed at high temperatures, ideally without network solder lines, were analyzed as laminate materials. Therefore, the materials broke at an angle of 90° under tensile load, as depicted in Fig. 11(a), since the filler filaments did not apply shear stress. The air cavities reduced the strength of the extrusion-free samples by the formation of micro-cracks under pressure and locally decreased physical cross-sectional areas of the material samples [46-48]. Also, Fig. 11 shows the parameters for the PEEK-cHAp, namely; the volumetric parameter and the peak count distribution of K-L transformations.

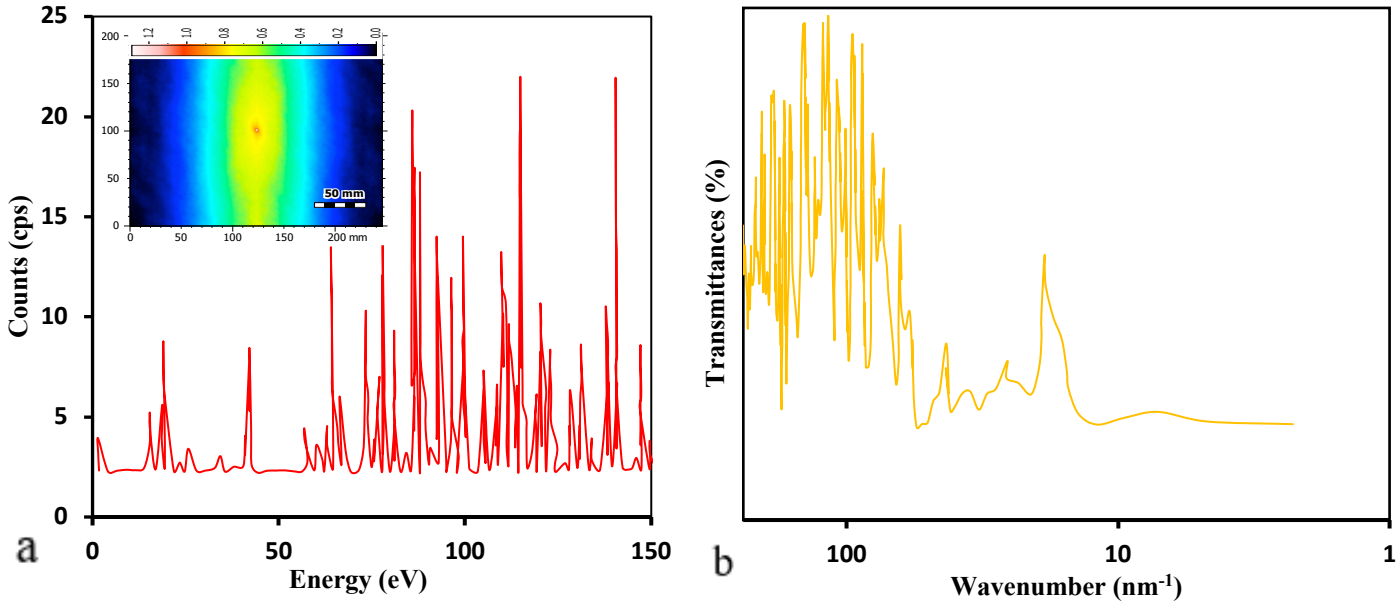

Fig. 11 The oriented PEEK-cHAp biocomposite, showing (a) energy dispersive X-ray analysis spectrum of a field sample and (b) differential scanning calorimetry (DSC) of Fourier-transform infrared spectroscopy (FTIR) spectrum for 3D printed and cast PEEK for a polarised infrared spectrum

The error bars, the brochures for each material, were modular in the selective laser; the maximum distribution was higher than the sample printed by the FDM technique with the SLS process. A high level of posture caused the variation. For example, it was observed with the SLS aluminum-filled polyamide (PA12-Al) samples [49-51], due to the lack of post-processing control that might have variable properties, significant changes in the strength and modulus of the synthetic fibers. The aluminum and polyamide particles have various physical properties. An efficient and stable combination can explain particle size, shape and density. Therefore, there was no distribution of these materials. Each layer caused changes in the flexural properties of the different samples. The coagulation of the material can be explained by the 3D printing of the PEEK resistors and the modulus discrepancies during the accumulation. Since the lamp surrounding the printed part controlled the ambient temperature, the cooling rate was probably lower than the aforementioned one. Porosity formation and random microbubbles could be another source of the differences in the materials, such as acrylonitrile butadiene styrene (ABS) samples printed with commercial FDM systems [52-54]. They exhibited a lowest variance when printed in the heat control room. The quality control standards determined by the biocompatibility test of medical devices required a thorough examination to verify the level of actual preparation for clinical use.

Conclusions

A new technique based on extrusion-compression molding and free-forming has been introduced to produce PEEK-cHAp biocomposite materials for bone implants. This innovative method allowed for better control of the bioactive phase distribution than conventional 3D printing of biopolymers, at a constant pressure of 0.39 MPa, waiting time of 20 minutes, temperature of 400 °C. The pore size was more significant than 200 racks interim and cHAp of 20 x 10 x 3 mm suitable for mold pressing, as a modification and an improvement to the previous studies. The practical technique supported the production of porous PEEK adjustment on the peak of the duct to be joined, with an average roughness of 0.4 μm in the PEEK matrix. At the same time, the PEEK-cHAp biocomposite material was characterized by good biocompatibility.

Also, PEEK biological activity was observed to be improved by adding HAp particles to the PEEK matrix for the preparation of a PEEK/cHAp biocomposite, using FDM technique. While the tensile properties and elastic modulus of the PEEK/cHAp composites with different HAp content ranging from 0-20 wt% were evaluated, a 15 wt% cHAp seemed to represent the ideal or optimum percentage weight. The *in vitro* assays test of the DMEM culture medium showed that the PEEK/cHAp composite showed better adhesion, proliferation, and cell activity than pure PEEK.

Finally, the result showed an excellent cell clotting through a combination of PEEK and cHAp composites. However, it exhibited a little reduction in mechanical properties due to the addition of the composite. Importantly, PEEK-cHAp biocomposite can survive by compression in a million period under a force of 30 N, which is the average weight that many parts of the body can exact on a bone at a time, without damaging its compression properties. This is very good in load-bearing applications. Undoubtedly, this study has provided a guide for the application of biomedical bone-implant compatibility, new material products, and future development that could demonstrate the potential preliminary evidence for a successful 3D printing of medical-grade PEEK, using an independent extrusion technique.

Authors Contributions

Bankole I. Oladapo: Conceptualization, Methodology, Software, Writing - original draft. **S. A. Zahedi:** Supervision, Formal analysis, Funding acquisition. **Sikiru O. Ismail:** Writing-review & editing, Supervision. **Francis Omigbodun:** Review & editing, Validation, Visualization, **Bowoto Oluwole:** Review & editing, Funding acquisition, Investigation. **Mattew A. Olawumi:** Data curation, Validation, Software. **Musa A. Muhammad:** Review & editing, Project administration, Software.

Ethical statement

The authors declare that there is no ethical issue; the study was conducted in full agreement with ethical standards. Also, the manuscript is neither under review nor published elsewhere.

Declaration of competing interest

We hereby affirm that there is no conflict of interest.

Acknowledgment

We appreciate the funding/financial support received from the Higher Education Innovation Fund (HEIF) of De Montfort University, Leicester, United Kingdom, under Research Project No.0043.06.

References

1. Edwards S, Werkmeister JA (2012) Mechanical evaluation and cell response of woven polyetheretherketone scaffolds. J Biomed Mater Res Part A100A:3326–3331
2. Oladapo BI, Zahedi SA, Chong S, Omigbodun FT, Malachi IO (2020) 3D printing of surface characterisation and finite element analysis improvement of PEEK-HAP-GO in bone implant. Int J Adv Manuf Tech 106:829-841
3. Ouyang L, Deng Y, Yang L, Shi X, Dong T, Tai Y, Yang W, Chen Z (2018) Graphene-oxide-decorated microporous polyetheretherketone with superior antibacterial capability and *in vitro* osteogenesis for orthopedic implant. Macromol Biosci 18:1800036
4. Kurtz SM, Devine JN (2008) PEEK biomaterials in trauma, orthopedic and spinal implants. Biomaterials 28:4845–4869

5. Wilmowsky CV, Vairaktaris E, Pohle D, Rechtenwald T, Lutz R, Munstedt H, Koller G, Schmidt M, Neukam W, Schlegel KA, Nkenke E (2008) Effects of bioactive glass and β-TCP containing three-dimensional laser sintered polyetheretherketone composites on osteoblasts *in vitro*. J Biomed Mater Res Part A 87:896–902
6. Oladapo BI, Zahedi SA, Vahidnia F, Ikumapayi OM, Farooq MU (2018) Three-dimensional finite element analysis of a porcelain crowned tooth. Beni-Suef Univ J Basic Appl Sci 7:461-464
7. Wang L, He S, Wu X, Liang S, Mu Z, Wei J, Deng F, Deng Y, Wei S (2014) Polyetheretherketone/nano-fluorohydroxyapatite composite with anticicrobial activity and osseointegration properties. Biomaterials 35:6758–6775
8. Shamsi-Sarband A., Zahedi S. A., Bakhshi-Jouybari M., Hossinipour S. J., Banabic D. (2012) Optimizitation of the pressure path in sheet metal hydroforming, Journal Proceedings Of The Romanian Academy, A 13: 351-359
9. Wang S, Lee JM, Yeong WY (2015). Smart hydrogels for 3D bioprinting. Int J Bioprint 1:3–14
10. Oladapo BI, Oshin EA, Olawumi AM (2020) Nanostructural computation of 4D printing carboxymethylcellulose (CMC) composite. Nano-Struct Nano-Obj 21:100423
11. Yang HY, Thompson I, Yang SF, Chi XP, Evans JRG, Cook RJ (2008) Dissolution scaffolds. J Mater Sci Med 19:3345–3353
12. Oladapo BI, Ismail SO, Zahedi M, Khan A, Usman H (2020) 3D printing and morphological characterisation of polymeric composite scaffolds. Eng Struct 216:110752
13. Yang HY, Yang S, Chi XP, Evans JRG, Thompson I, Cook RJ, Robinson P (2008) Sintering behaviour of calcium phosphate filaments for use as hard tissue scaffolds. J Europ Ceram Soc 28:159–167
14. Li S., Zahedi SA., Silberschmidt V., (2017), Numerical Simulation of Bone Cutting: Hybrid SPH-FE Approach Numerical Methods and Advanced Simulation in Biomechanics and Biological Processes, 187-201
15. Yang S, Yang H, Chi X, Evans JRG, Thompson I, Cook RJ, Robinson P (2008) Rapid prototyping of ceramic lattices for hard tissue scaffolds. Mater Des 29:1802–1809
16. Adeoye AOM, Kayode JF, Oladapo BI, Afolabi SO (2017) Experimental analysis and optimization of synthesized magnetic nanoparticles coated with PMAMPC-MNPs for bioengineering application. St. Petersburg Polytech Univ J Phys Math 3:333-338
17. Zhao Y, Wong HM, Wang W, Li P, Xu Z, Chong EYW, Yan CH, Yeung KWK, Chu PK (2013) Cytocompactibility, osseointegration, and bioactivity of three-dimensional porous and nanostructure network on polyetheretherketone. Biomaterials 34:9264–9277
18. Zahedi S.A., Demiral M., Roy A., Silberschmidt V.V., (2017) FE/SPH modelling of orthogonal micro-machining of fcc single crystal, Computational materials science 78, 104-109
19. Ziemian C, Sharma M, Ziemian S (2012) Anisotropic mechanical properties of ABS parts fabricated by fused deposition modelling. In: M. Gokcek, ed. Mechanical Engineering. Rijeka: InTech, 2012; Chapter 7:159–80
20. Balogun VA, Oladapo BI (2016) Electrical energy demand modeling of 3D printing technology for sustainable manufacture. Int J Eng 29:954-961
21. Ma R, Tang T (2014) Current strategies to improve the bioactivity of PEEK. Int J Mol Sci 15:5426–5445
22. Li X, He J, Bian W, Li Z, Zhang W, Li D, Snedeker JG (2014) A novel silk-based artificial ligament and tricalcium phosphate/polyether ether ketone anchor for anterior cruciate ligament reconstruction – Safety and efficacy in a porcine model. Acta Biomater 10:3696–3704

23. Oladapo BI, Victor AA, Elemure IE (2019) Microstructural 4D printing investigation of ultra-sonication biocomposite polymer. J King Saud Univ Eng Sci 1-7
24. Ma R, Tang S, Tan H, Qian J, Lin W, Wang Y, Liu C, Wei J, Tang T (2014) Preparation, characterization, *in vitro* bioactivity, and cellular responses to a polyetheretherketone bioactive composite containing nanocalcium silicate for bone repair. ACS Appl Mater Interf 6:12214–12225
25. Omigbodun FT, Oladapo BI, Bowoto OK, Adeyekun FP (2019) Modelling detection of magnetic hysteresis properties with a microcontroller. Inte J Eng Trends Technol 67:5-12
26. Wang L, He S, Wu X, Liang S, Mu Z, Wei J, Deng F, Deng Y, Wei S (2014) Polyetheretherketone/nano-fluorohydroxyapatite composite with antimicrobial activity and osseointegration properties. Biomaterials 35:6758–6775
27. Zahedi S.A., Kodsi C., Berto F., (2019) Numerical predictions of U-notched sample failure based on a discrete energy argument, Theoretical and Applied Fracture Mechanics 100, 298-306
28. Lu T, Wen J, Qian S, Cao H, Ning C, Pan X, Jiang X, Liu X, Chu PK (2015) Enhanced osteointegration on tantalum-implanted polyetheretherketone surface with bone-like elastic modulus. Biomaterials 51:173–183
29. Xu A, Liu X, Gao X, Deng F, Deng Y, Wei S (2015) Enhancement of osteogenesis on micro/nano-topographical carbon fibre-reinforced polyetheretherketone–nanohydroxyapatite biocomposite. Mater Sci Eng C 48:592–598
30. Oladapo BI, Malachi IO, Malachi OB, Elemure IE, Olawumi AM (2020) Nano-structures of 4D morphology surface analysis of $C_{17}Mn_{0.6}P_{0.1}S_{0.07}$ (SAE 1045) wear. Nano-Struct Nano-Obj 22:100433
31. Eltorai AE, Nguyen E, Daniels AH (2015) Three-dimensional printing in orthopedic surgery. Orthopedics 38:684-687
32. Wang H, Xu M, Zhang W, Kwok DTK, Jiang J, Wu Z (2010). Mechanical and biological characteristics of diamond-like carbon coated poly aryl-ether-ether-ketone. Biomaterials 31:8181–8187
33. Gibbs DM, Vaezi M, Yang S, Oreffo RO (2014) Hope versus hype: What can additive manufacturing realistically offer trauma and orthopaedic surgery? Regen Med 9:535-549
34. Oladapo BI, Daniyan IA, Ikumapayi OM, Malachi OB, Malachi IO (2020) Microanalysis of hybrid characterization of PLA/cHA polymer scaffolds for bone regeneration. Polym Test 83:106341
35. Martelli N, Serrano C, van den Brink H, Pineau J, Prognon P, Borget I, El Batti S (2016) Advantages and disadvantages of 3-dimensioanl printing in surgery: A Systematic review. Surgery 159:1485-1500
36. Zahedi A, Demiral M, Roy A, Babitsky VI, Silberschmidt VV (2012) Indentation in fcc single crystals Solid State Phenomena 188: 219-225
37. Provigil E, Leong JJH, Kalaskar DM (2017) Application of 3D printing in the mangament of severe spinal conditions. Proc Inst Mech Eng Part H J Eng Med 231:471-486
38. Oladapo BI, Adeoye AOM, Ismail M (2018) Analytical optimization of a nanoparticle of microstructural fused deposition of resins for additive manuf. Compos Part B Eng 150:248-254
39. Oladapo BI, Obisesan OB, Bowoto O, Victor AA, Hazrat U, Affan K (2020) Mechanical characterization of a polymeric scaffold for bone implant. J Mater Sci 55:9057-9069
40. Oladapo BI, Zahedi SA, Chaluvadi SC, Bollapalli SS, Ismail M (2018) Model design of a superconducting quantum interference device of magnetic field sensors for magnetocardiography. Biomed Sig Proc Cont 46:116-120
41. Tang SM, Cheang P, Abu Bakar MS, Khor KA, Liao K (2004) Tensiontension fatigue behaviour of hydroxyapatite reinforced polyetheretherketone composites. Int J fatig 26:49–57

42. Oladapo BI, Zahedi SA, Omigbodun FT, Oshin EA, Adebiyi VA, Malachi OB (2019) Microstructural evaluation of aluminum alloy A365 T6 in machining operation. J Mater Res Technol 8:3213-3222

43. Tafaoli-Masoule M, Shakeri M, Zahedi SA, Seitz H, Vaezi M (2019) 3D printing of PEEK-based medical devices Transactions on Additive Manufacturing Meets Medicine 1 (1)

44. Abu Bakar MS, Cheng MHW, Tang SM, Yu SC, Liao K, Tan CT, Khor KA, Cheang P (2003) Tensile properties, tension–tension fatigue and biological response of polyetheretherketone–hydroxyapatite composites for load-bearing orthopedic implants. Biomaterials 24:2245–2250

45. Tlegenov Y, Wong YS, Hong G-S (2017) A dynamic modelfor nozzle clog monitoring in fused deposition modelling. Rapid, Prototyp J 23:391–400

46. Vaezi M, Yang S (2015) Extrusion-based additive manufacturing of PEEK for biomedical applications. J Virt Phys Prototyp 10:123–135

47. Oladapo BI, Zahedi SA, Adeoye AOM (2019) 3D printing of bone scaffolds with hybrid biomaterials. Compos Part B Eng 158:428-436

48. Geng P, Zhao J, Wu W, Ye W, Wang Y, Wang S, Zhang S (2019) Effects of extrusion speed and printing speed on the 3D printing stability of extruded PEEK filament. J Manuf Proc 37:266-273

49. Deng Y, Yang L, Huang X, Chen J, Shi X, Yang W, Hong M, Wang Y, Dargusch MS, Chen Z-G (2018) Dual ag/zno-decorated micro-/nanoporous sulfonated polyetheretherketone with superior antibacterial capability and biocompatibility via layer-by-layer self-assembly strategy. Macromol Biosci 18:1800028

50. Ding S, Zou B, Wang P, Ding H (2019) Effects of nozzle temperature and building orientation on mechanical properties and microstructure of PEEK and PEI printed by 3D-FDM. Polym Test 78:1-9

51. Ijagbemi CO, Oladapo BI, Campbell HM, Ijagbemi CO (2016) Design and simulation of fatigue analysis for a vehicle suspension system (VSS) and its effect on global warming. Procedia Eng 159:124-132

52. Wang P, Zou B, Xiao H, Ding S, Huang C (2019) Effects of printing parameters of fused deposition modelling on mechanical properties, surface quality, and microstructure of PEEK. J Mater Proc Technol 271:62-74

53. Zhong G, Vaezi M, Liu P, Pand L, Yang S (2017) Characterisation approach on the extrusion process of bioceramics for the 3D printing of bone tissue engineering scaffolds. Ceram Int 43:13860-13868

54. Ma R, Guo D (2019) Evaluating the bioactivity of a hydroxyapatite-incorporated polyetheretherketone biocomposite. J Orthop Surg Res 14:1-13

55. Deng L, Deng Y, Xie K (2017) AgNPs-decorated 3D printed PEEK implant for infection control and bone repair. Colloids Surf B Biointerfaces 160:483–492

56. Wang L, Weng L, Song S, Sun Q (2010) Mechanical properties and microstructure of polyetheretherketone–hydroxyapatite nanocomposite materials. Mater Lett 64:2201-2204

57. Fan JF, Tsui CP, Tang CY, Chow CL (2004) Influence of interphase layer on the overall elasto-plastic behaviors of HA/PEEK biocomposite. Biomaterials 25:5363–5373